
Early Transferability of Adversarial Examples in Deep Neural Networks

Oriel BenShmuel
Faculty of Math&CS
Weizmann Institute of Science
Israel
oriel.benshmuel@weizmann.ac.il

Abstract

This paper will describe and analyze a new phenomenon that was not known before, which we call “Early Transferability”. Its essence is that the adversarial perturbations transfer among different networks even at extremely early stages in their training. In fact, one can initialize two networks with two different independent choices of random weights and measure the angle between their adversarial perturbations after each step of the training. What we discovered was that these two adversarial directions started to align with each other already after the first few training steps (which typically use only a small fraction of the available training data), even though the accuracy of the two networks hadn’t started to improve from their initial bad values due to the early stage of the training. The purpose of this paper is to present this phenomenon experimentally and propose plausible explanations for some of its properties.

1 Introduction

Previous findings had demonstrated the surprising fact that tiny adversarial perturbations could fool trained deep neural networks [29, 3]. The distorted images, known as “adversarial examples” have become a major concern for machine learning practitioners since they enable attackers to fool even the best trained deep neural networks by slightly modifying the input in a way that is not perceptible to humans. This fact naturally raised the curiosity of the deep learning community [21, 15, 18, 4, 33, 2, 10, 5]. In the same paper [29], Szegedy et al. also mentioned the “cross-generalization” property, where the same adversarial example can usually fool a wide variety of networks, which may differ in architecture and even disjoint datasets. This poorly understood phenomenon is called “Transferability”.

Shortly afterward, it was discovered that different models with similar decision boundaries enable transferability [32]. In fact, a strong correlation between adversarial directions of the two models (concerning the same sample) implies transferability (but not necessarily vice versa). Generally, a strong correlation between two random vectors is very unlikely due to the high dimension of the input space (accurate measurements appear in Appendix A).

Black-box adversarial attacks rely on transferability [20]. By attacking a surrogate model that the attacker trained, we get adversarial examples that could fool the original network with high probability (without further information concerning the parameters of the original model itself).

Studied discuss the nature of transferability by estimating the space of adversarial examples [32] or alternatively introducing new mental images that aim to explain the phenomenon, such as robust and non-robust features [15] or the linear nature of neural networks [9, 12]. Another series of studies discuss defense methods [22, 19, 34, 23, 25, 14] and attack methods [1, 8, 11, 6, 7, 31].

The adversarial perturbations of the same image, computed by using two models with random weights (before the training phase), are random as well and tend to be perpendicular (as explained in Appendix A and observed in sections 3, 4.5, and Appendix C). A reasonable assumption might be that transferability occurs after the networks learn some features of the data, which usually takes several epochs in non-trivial datasets.

This paper will describe and explain a new phenomenon that was not known before. Its occurrence influences and emphasizes the transferability effect at the very beginning of the learning process with possible long-term consequences. We call this occurrence “Early Transferability”, and although it is characterized by the same behavior as the general notion of transferability as defined above, it is caused by reasons that are relevant mainly during the early stages of the training phase and has additional and counter-intuitive properties. First, we describe the new phenomenon and its counter-intuitive properties with an extensive explanation of the goal of presenting it. Then, we experimentally present the occurrence using multiple different settings. Finally, we propose a partial explanation for the occurrence while we try to understand the impact of each network’s parameters concerning the new phenomenon.

2 Early transferability

Even though the transferability occurrence is still vague, typically, we would expect it to happen as part of the process of learning the data. In particular, it could only occur after some properties of the data were learned, which usually takes a few epochs in non-trivial datasets (as a function of the data complexity). This is not the case for early transferability.

2.1 Early transferability and complex datasets

Naturally, complex datasets require advanced architectures and more epochs for the network to perform well, as opposed to basic datasets. Assuming the general notion of transferability addresses trained networks, we expect the effect to evolve as part of the network’s learning process. This assumption points to a difference between the transferability evolution using complex datasets and basic datasets.

In contrast, the early transferability effect has no relation to the ability of the network to learn and generalize. It might happen even *before* the network started to improve its initial 50% accuracy, or even in the first *step* (which is based on a tiny subset of the data as a function of the batch size), rather than after several *epochs*. As a result, early transferability might occur even when the data is highly complex, the current architecture could not learn it, or even if the data is not learnable at all (for example, there is no semantic difference between classes, or alternatively, the data is built from random noise).

2.2 Long-term effect

As mentioned before, the impact of early transferability might differ as a function of the train settings. Even though early transferability occurs in the early stages of the training, it might influence the long-term training and the long-term transferability due to the initial impact of the effect (for further details, see section 4.5).

2.3 Controlling early transferability

This paper will explain and experimentally demonstrate the influence of early transferability for different types of hyper-parameters. Understanding its properties and behavior could imply the parameters that influence it. Controlling these parameters helps us emphasize or reduce this effect or generally be aware of it.

2.4 The goal of early transferability

Early transferability has three main goals:

1. *Prevent confusion*: Showing this phenomenon aims to prevent confusion between traditional transferability and early transferability. Being aware of early transferability might shed light

on various fields of research regarding transferability. Studies that discuss transferability could reach better conclusions when isolating the traditional transferability effect. For example, when investigating the relationship between transferability and complex datasets or the evolution of this occurrence during training.

2. *Reliability*: When studying transferability, conclusions might include biased results toward early transferability rather than the traditional transferability. It is essential to address it since the effect of early transferability can be controlled by the input hyper-parameters and, therefore, could create a massive impact on the results (in the long term as well). We consider the early transferability effect as a nonobjective effect, which was influenced by the trainer. We would address the traditional transferability as the objective effect that evolves naturally and independently of the inserted parameters.

Moreover, black-box attacks are more reliable when based on traditional transferability rather than early transferability since early transferability assumes emphasized effect using some set of parameters. In contrast, using different parameters might cause a weaker effect. In the process of demonstrating black-box attacks, we might choose the reference model ourselves. At the same time, our experimental results and conclusions might be biased due to a more substantial early transferability effect rather than a different choice of parameters that could massively weaken the presented results.

3. *What to do?* Being aware of this effect might lead to a better understanding of how transferability behaves. However, more importantly, understanding it helps to reduce (or emphasize) the effect in order to achieve better conclusions (or generate new forms of attacks).

3 Experimental results

In this section, we present the “Early Transferability” effect by generating quantitative experiments based on a wide range of settings.

3.1 Framework

The following properties in the analysis will help us witness the transferability in the very early stages of the training:

1. *Steps*: Early transferability refers to the type of transferability that happens already in the early stages of the training. In order to test that, the experiments will use “zoom-in” observations of the training process, such that the provided details are shown in scale of steps (where each optimizer step includes only one batch from the training set) rather than in scale of epochs (where each epoch includes the entire train set).
2. *Angles*: For each step, we compute the angle between the adversarial directions of the two models for each sample. The displayed result is an average of over 100 samples from the *test set* (to emphasize that this kind of transferability has nothing to do with the specific train images that the model observed). We are interested in deviations from the 90° angle expected for pairs of random vectors. In some cases, the correlation was negative. Therefore, for each angle $a > 90^\circ$, we will display $180^\circ - a$.
3. *Accuracy*: One of the mentioned claims states that early transferability is unrelated to the accuracy of the model. Specifically, the model might improve its test accuracy on the data after every few steps, or (in more complex cases) it might stay steady (at 50% accuracy) for many steps. In this set of experiments, we show that we might get an extremely high transferability effect, even in the cases where the model hasn’t learned anything yet (in terms of test accuracy). Therefore we will display the test accuracy of each model.

Generally, we will use Adam optimizer [16]. The same effect is true for the RMSprop optimizer [30], and it also appears when using SGD [27] (with and without momentum [28]). Still, for SGD, the effect is smaller due to reasons that appear in subsection 4.4. Additionally, we are using different shuffles for the dataset in each of the two models to show that the effect occurs even when we train the models on entirely *different* images (expressed with disjoint batches) during the early steps. The experiments were executed using GPU “Tesla K80”.

3.2 Results

In Figure 1, we can observe the results of a pair of deep fully-connected networks (according to the “Deep network” architecture mentioned in Appendix B) trained to classify between *Cat* and *Dog* of the CIFAR10 dataset [17] with a learning rate of $1e-2$ and batch size of 128 under the described analysis. In the graph, we can see that the starting point of the networks, when they are randomly initialized, produces an angle of nearly 90° between the adversarial directions as should be in high dimensional space, while both of the accuracy values of the networks are 50% as expected. Observing the same values after the first step shows us a drastic change in the angle to less than 40° , while the accuracy is still steady at 50% (it will start improving only at steps 3 and 10 of the two networks, respectively).

As discussed earlier, an average angle between randomly sampled vectors (in high dimensions) should be very close to 90° . At the same time, the standard deviation is small as a function of the space dimension (for more details, see Appendix A). Based on that, even minor deviations from the mean value are significant and extremely unlikely.

In the presented case, we use a small batch size (128) compared to the entire dataset and especially compared to the input space dimension, which is 3072. This ratio leaves many degrees of freedom for the network to “learn” from the given data and change its weights accordingly, and yet the minimally trained networks are already transferable.

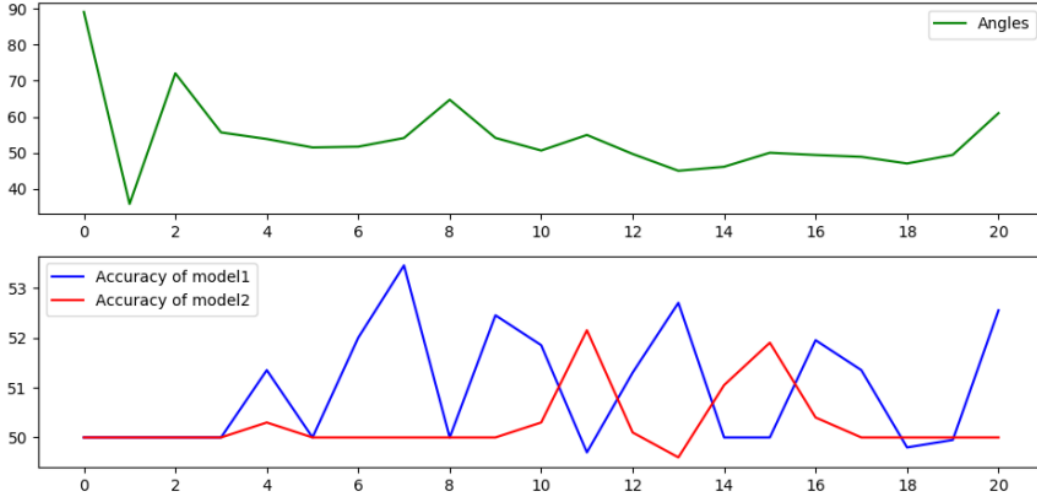


Figure 1: The “Early Transferability” effect by “zooming in” into the beginning of the learning process.

The effect of early transferability is not unique to fully-connected networks. The phenomenon also exists in convolutional networks. In Figure 2, we can observe the same analysis (with similar categories) using Architecture B (convolutional network, see Appendix B), batch size of 128, and learning rate of $1e-3$.

Similarly, the effect also occurs for complex datasets such as the ImageNet dataset [24]. In Figure 3, we present the described analysis using the VGG11 network [26] trained to classify *Goldfish* and *White Shark* from the ImageNet dataset, with a batch size of 16 and a learning rate of $1e-3$.

For additional experiments with different settings, see Appendix C.

4 The first steps of the training process

This section proposes a simple explanation based on some interesting results for the most basic case, fully-connected networks trained with SGD optimizer, which leads to a high-level understanding of early transferability. In particular, the models were trained with *disjoint* batches (randomly sampled

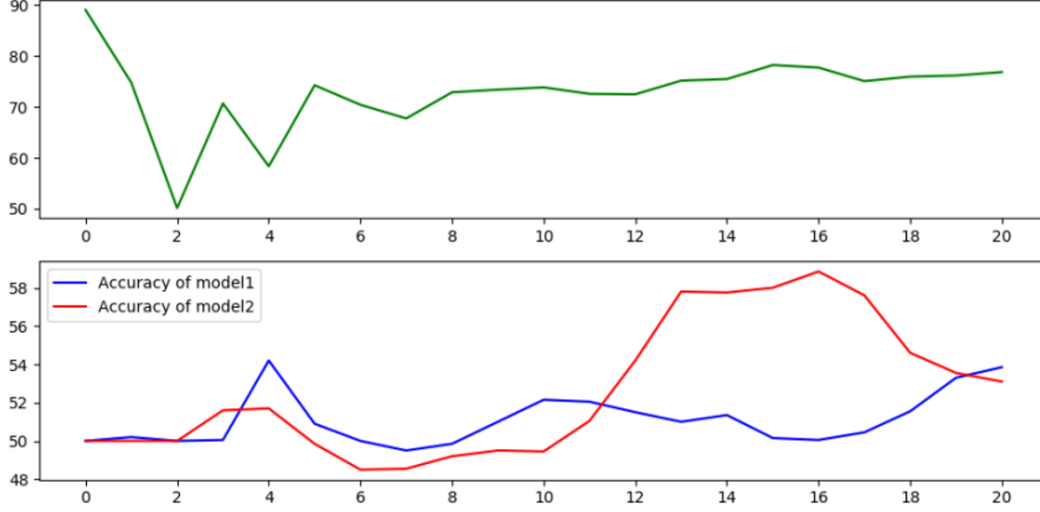


Figure 2: The “Early Transferability” effect using CNN.

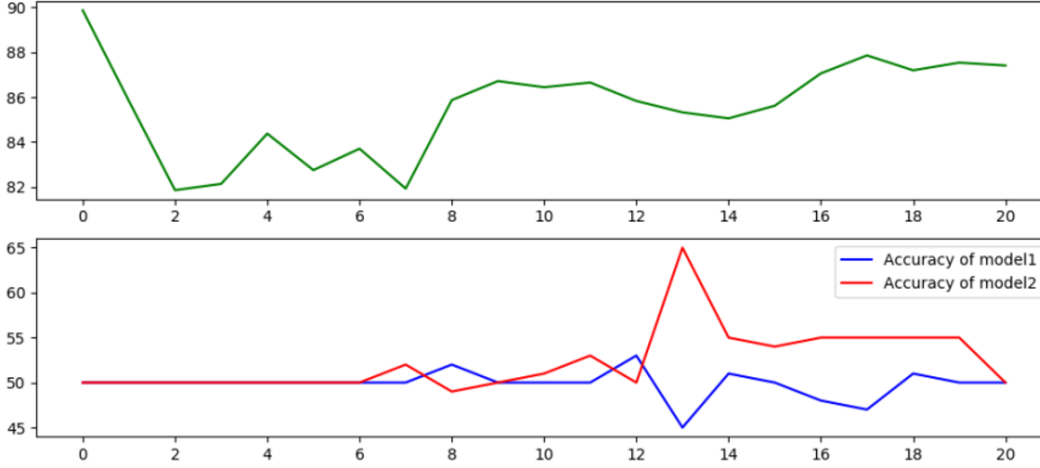


Figure 3: The “Early Transferability” effect using the vgg11 network trained with ImageNet.

from the dataset). In subsection 4.4, we will elaborate on optimizers that might emphasize this effect and the possible long-term influence (in subsection 4.5).

4.1 Notation

We denote by $\theta_l[j]$ the j -th row in the weights matrix θ_l from size $k \times n$ (where $0 \leq j < k$) of layer number l in the network. We also denote by $\partial\theta_l[j]$ the change in the weights $\theta_l[j]$ when calculating the gradient of the loss function with respect to the weights.

For the sake of simplicity, we usually address $\{\theta_l[j]\}_{0 \leq j < k}$ and $\{\partial\theta_l[j]\}_{0 \leq j < k}$ as “vectors of weights” and “vectors of updates”, respectively.

4.2 Discussion

For a pair of randomly initialized networks, we get almost perpendicular adversarial directions (based on similar input). This angle between the two adversarial vectors is typical for the high-dimensional input space (as we explain in Appendix A). However, the experimental results point to correlated adversarial vectors, sometimes even after the first step. The only change we made in the initial settings is updating the weights of the networks. Following that, we can observe the weights of a

fully-connected network as a set of vectors rather than a matrix of weights, such that each vector represents the relation between a neuron of the following layer and the entire set of weights connecting it to the current layer.

During the first steps of the training process, we encountered the following occurrences, which we experimentally support in this section:

1. Focusing on the first layer of each network, where the “vectors of updates” of the first network are $A = \{\partial\theta_1[j]\}_{0 \leq j < k}$ and the “vectors of updates” of the second network are $B = \{\partial\theta'_1[j']\}_{0 \leq j' < k'}$, we get that each pair of vectors from the united set $A \cup B$ is highly correlated with high probability. In particular, it occurs even when using a different batch of images for each model and a non-linear objective.
2. For a fully-connected network with a correlated set of “vectors of weights”, we get that the adversarial direction is correlated to them as well. In fact, the adversarial direction will be correlated to each one of the vectors in the set with high probability.

Combining these two properties together, a large enough impact (depending on the learning rate, batch size, and optimizer) of the “vectors of updates” will convert the initial vectors of weights to be correlated as well, and therefore, the networks will generate correlated adversarial directions with high probability.

Additionally, for a relatively “slow” optimizer (which might have a small impact on the weights update in the first steps), such as SGD, the effect is smaller and requires a higher learning rate to witness the effect. In contrast, for relatively “aggressive” optimizers, such as the Adam optimizer, the effect will be much more significant and will clearly appear even when using relatively small learning rates (more information, see subsection 4.4).

Concluding all this new information (which we support experimentally), we get that for the right amount of impact of the weights update, the adversarial vectors are correlated with high probability.

4.3 Experimental support

For the fully-connected architectures mentioned in Appendix B, the categories *Cat* and *Dog* of the dataset CIFAR10 [17], the negative log-likelihood loss function, and for a single training step based on a *different* batch of images for each model, we will check the correlations between $\partial\theta_1[j_1]$ and $\partial\theta_1[j_2]$ (for $0 \leq j_1 \neq j_2 < k$) among each model separately (using only one model) and between two different models (for similar architectures and different architectures). For convenience, we will ignore the correlation signs by transforming angles $a > 90^\circ$ to be $180^\circ - a$ since we are only interested in deviations from the expected 90° angle. The weights of the first layer are θ_1 of size $k \times n$ for the first model and θ'_1 of size $k' \times n$ for the second model.

For a single step, batch size 30, input space dimension $n = 3072$, and the network’s fully-connected architectures mentioned in Appendix B, the results appear in Table 1 show the average angles based on the following description:

1. *Angles of model 1*: Average angle between $\partial\theta_1[j_1]$ and $\partial\theta_1[j_2]$ ($0 \leq j_1 \neq j_2 < k$).
2. *Angles of model 2*: Average angle between $\partial\theta'_1[j_1]$ and $\partial\theta'_1[j_2]$ ($0 \leq j_1 \neq j_2 < k'$).
3. *Angles between models*: Average angle between $\partial\theta_1[j_1]$ and $\partial\theta'_1[j_2]$ for any valid combination of indices.

Table 1: The average angle between the “vectors of updates” ($n = 3072$).

Architecture	Angles of model 1	Angles of model 2	Angles between models
Shallow networks	72.83°	74.22°	73.74°
Deep networks	75.40°	75.29°	75.92°
Deep Vs Shallow	73.45°	74.37°	74.02°

For the same settings, where the generated “vectors of updates” are correlated, training the network with a *significant* learning rate (such that the initial weights are negligible compared to the derivatives)

for a single step will generate new weights $\bar{\theta}_1, \bar{\theta}'_1$ that will be significantly biased toward $\partial\theta_1, \partial\theta'_1$, respectively. Table 2 shows the following:

1. *Adversarial angles of model 1*: Average angle between $\bar{\theta}_1[j]$ ($0 \leq j < k$) and the adversarial vector w.r.t the first model (average over 100 adversarial vectors).
2. *Adversarial angles of model 2*: Average angle between $\bar{\theta}'_1[j]$ (for $0 \leq j < k'$) and the adversarial vector w.r.t the second model (average over 100 adversarial vectors).

Table 2: The angle between the “vectors of weights” of each model and the adversarial vectors.

Architecture	Adversarial angles of model 1	Adversarial angles of model 2
Shallow networks	68.31°	67.51°
Deep networks	72.78°	72.61°
Deep Vs Shallow	66.01°	66.9°

Based on Appendix A, for the input dimension of 3072, the angles we expect from each cell in Tables 1 and 2 should be $\sim 88.96^\circ$, and the probability of getting an angle of $\sim 70^\circ$ is extremely low.

4.4 Optimizers

The above explanation (in this section) was demonstrated using stochastic gradient descent steps, known as “SGD” [27], where we update the weights in iteration t as follows:

$$\theta^{t+1} = \theta^t - lr \cdot \partial\theta^t$$

Another commonly used optimizer is “Adam” [16], with the following iterative optimization:

$$\begin{aligned} \mathcal{V}^{t+1} &= \beta_1 \cdot \mathcal{V}^t + (1 - \beta_1) \cdot \partial\theta^t \\ \mathcal{S}^{t+1} &= \beta_2 \cdot \mathcal{S}^t + (1 - \beta_2) \cdot (\partial\theta^t)^2 \\ \mathcal{S}_c^{t+1} &= \mathcal{S}^{t+1} / (1 - \beta_2^{t+1}), \mathcal{V}_c^{t+1} = \mathcal{V}^{t+1} / (1 - \beta_1^{t+1}) \\ \theta^{t+1} &= \theta^t - lr \cdot \frac{\mathcal{V}_c^{t+1}}{\sqrt{\mathcal{S}_c^{t+1} + \epsilon}} \end{aligned}$$

For the usually predetermined constants $\beta_1 = 0.9, \beta_2 = 0.999, \epsilon = 1e - 8$, where the standard initial conditions are $\mathcal{V}^0 = 0, \mathcal{S}^0 = 0, t = 0$, we get that the first step results in the following expression:

$$\begin{aligned} \mathcal{V}^1 &= 0.1\partial\theta^0, \mathcal{S}^1 = 0.001(\partial\theta^0)^2 \\ \mathcal{V}_c^1 &= \partial\theta^0, \mathcal{S}_c^1 = (\partial\theta^0)^2 \\ \theta^1 &= \theta^0 - lr \frac{\partial\theta^0}{\sqrt{(\partial\theta^0)^2 + \epsilon}} \sim \theta^0 - lr \frac{\partial\theta^0}{|\partial\theta^0|} \end{aligned}$$

We get that the expression $\frac{\partial\theta^0}{|\partial\theta^0|}$ (up to the small error generated by ϵ) is a vector with the elements $\pm 1, 0$ (independently of the metric we are using - $\ell_0, \ell_1, \ell_2, \ell_\infty$). The earlier the step is, the closer expression to $\frac{\partial\theta^0}{|\partial\theta^0|}$ we’ll get.

This occurrence leads to a reasonable explanation for the emphasized effect of early transferability using Adam optimizer. The weights’ update for Adam is $lr \frac{\partial\theta^0}{|\partial\theta^0|}$, where the stochastic gradient step is $lr \cdot \partial\theta^0$. Typically, the values of $|\partial\theta^0|$ are much smaller than 1 in the traditional SGD. Therefore we get (excluding zero elements):

$$\left| lr \frac{\partial\theta^0}{|\partial\theta^0|} \right| > \left| lr \partial\theta^0 \right|$$

Overall the update using Adam optimizer is much more “aggressive” than the update of SGD. Since early transferability depends on the values of the derivatives of the weights, a larger step will emphasize the effect. Therefore Adam optimizer could use a lower learning rate in order to create the same effect compared to SGD.

4.5 The influence on the general training process

According to the above analysis (section 4), a massive influence of the weights’ update might create a noticeable occurrence of early transferability. The general idea of early transferability concerns the weights’ update of the two given networks. We experimentally found that the vectors of updates are unexpectedly correlated. These correlated vectors of updates might lead the state of the two networks to be very close to the same local minima after very few steps of the training process. It might increase the probability of the networks converging to a similar solution in the long-term perspective of the training. Therefore, we might suspect that early transferability might influence long-term training. In particular, a prominent occurrence of early transferability in the initial steps might increase the long-term transferability.

We present a similar analysis to the one described in section 3, but in the current analysis, we desire to capture the long-term properties of the training process. Therefore, we measure the horizontal timeline of the training with epochs rather than with steps. Moreover, we want to present the long-term evolution using two settings. One of the settings has a significant occurrence of the early transferability effect (observed in the early stages). The other has a low occurrence of the effect. To avoid any other factor that might influence the experiment, we use similar parameters for both cases, except for one parameter, the learning rate.

In Figures 4 and 5, we use a batch size of 128, Adam optimizer, and CIFAR10 dataset [17] with the categories *Airplane* and *Automobile*. We use Architecture B, which appears in Appendix B. The learning rates used in Figures 4 and 5 are $1e-2$, $1e-4$, respectively. We can clearly see that both models converged and are in a steady-state. However, the top graph presented in both figures points to a massive difference in the angle between the perturbations, while the bottom graphs in both figures show approximately the same results. The difference between the long-term transferability occurrences might be explained by the different impacts of the early transferability effects during the initial stages of the training.

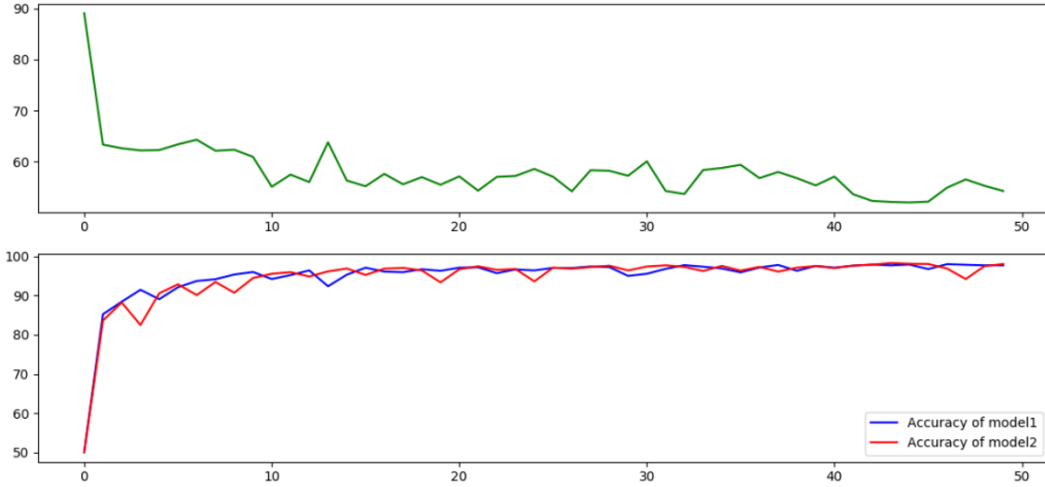


Figure 4: Long-term influence using epochs timeline. Learning rate of $1e-2$

Additional experiments appear in Appendix C.

5 Limitations

Early transferability might occur for models trained with reasonable hyperparameters, as demonstrated in this paper. Yet, the consequences might change for different tuning. In particular, for optimizers such as SGD, the effect might occur only for a significant learning rate as opposed to Adam optimizer. Additionally, the effect occurs in the best manner when the hyperparameters of the reference and target model are similar (even though identical parameters are not required).

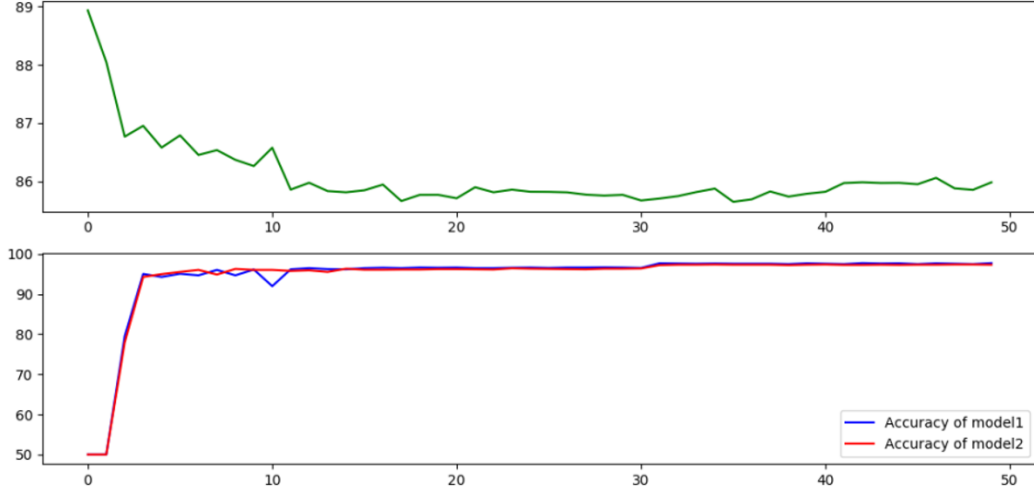


Figure 5: Long-term influence using epochs timeline. Learning rate of $1e - 4$

6 Conclusion

Our findings provide evidence for an unknown and counter-intuitive phenomenon. One of the key insights behind this is the unexpectedly early stages, in which the adversarial directions start to align with each other. We have conducted a supportive experimental analysis for several architectures (fully-connected, convolutional, residual), datasets (CIFAR10, ImageNet), and many hyperparameters. Our findings prompt us to view transferability as a combined occurrence of “early transferability” and “traditional transferability”, where the first one could be reduced or emphasized by different (but reasonable) hyperparameters. In addition, we explain why some optimizers might generate a greater impact than others. Our experimental results and proposed explanations shed light on various factors such as the possible long-term influence of “early transferability” during the training process and the unrelated impact of this effect w.r.t. the data complexity, or the ability of the network to learn. In section 2.4, we present the essence of this effect and hope that the discovered occurrence will reduce the mysteries surrounding “Transferability”.

References

- [1] N. Akhtar and A. Mian. Threat of adversarial attacks on deep learning in computer vision: A survey. *IEEE Access*, 6:14410–14430, 2018.
- [2] A. Athalye, N. Carlini, and D. Wagner. Obfuscated gradients give a false sense of security: Circumventing defenses to adversarial examples. In *International conference on machine learning*, pages 274–283. PMLR, 2018.
- [3] B. Biggio, I. Corona, D. Maiorca, B. Nelson, N. Šrndić, P. Laskov, G. Giacinto, and F. Roli. Evasion attacks against machine learning at test time. In *Joint European conference on machine learning and knowledge discovery in databases*, pages 387–402. Springer, 2013.
- [4] N. Carlini and D. Wagner. Adversarial examples are not easily detected: Bypassing ten detection methods. In *Proceedings of the 10th ACM workshop on artificial intelligence and security*, pages 3–14, 2017.
- [5] N. Carlini and D. Wagner. Audio adversarial examples: Targeted attacks on speech-to-text. In *2018 IEEE Security and Privacy Workshops (SPW)*, pages 1–7. IEEE, 2018.
- [6] S. Cheng, Y. Dong, T. Pang, H. Su, and J. Zhu. Improving black-box adversarial attacks with a transfer-based prior. In H. Wallach, H. Larochelle, A. Beygelzimer, F. d’Alché-Buc, E. Fox, and R. Garnett, editors, *Advances in Neural Information Processing Systems*, volume 32. Curran Associates, Inc., 2019.
- [7] H. Dai, H. Li, T. Tian, X. Huang, L. Wang, J. Zhu, and L. Song. Adversarial attack on graph structured data. In J. Dy and A. Krause, editors, *Proceedings of the 35th International*

- Conference on Machine Learning*, volume 80 of *Proceedings of Machine Learning Research*, pages 1115–1124. PMLR, 10–15 Jul 2018.
- [8] Y. Dong, F. Liao, T. Pang, H. Su, J. Zhu, X. Hu, and J. Li. Boosting adversarial attacks with momentum. In *Proceedings of the IEEE Conference on Computer Vision and Pattern Recognition (CVPR)*, June 2018.
 - [9] I. J. Goodfellow, J. Shlens, and C. Szegedy. Explaining and harnessing adversarial examples, 2015.
 - [10] K. Grosse, N. Papernot, P. Manoharan, M. Backes, and P. McDaniel. Adversarial examples for malware detection. In *European symposium on research in computer security*, pages 62–79. Springer, 2017.
 - [11] C. Guo, J. Gardner, Y. You, A. G. Wilson, and K. Weinberger. Simple black-box adversarial attacks. In K. Chaudhuri and R. Salakhutdinov, editors, *Proceedings of the 36th International Conference on Machine Learning*, volume 97 of *Proceedings of Machine Learning Research*, pages 2484–2493. PMLR, 09–15 Jun 2019.
 - [12] Y. Guo, Q. Li, and H. Chen. Backpropagating linearly improves transferability of adversarial examples. *Advances in Neural Information Processing Systems*, 33:85–95, 2020.
 - [13] K. He, X. Zhang, S. Ren, and J. Sun. Deep residual learning for image recognition. In *Proceedings of the IEEE conference on computer vision and pattern recognition*, pages 770–778, 2016.
 - [14] C.-H. Ho and N. Nvasconcelos. Contrastive learning with adversarial examples. *Advances in Neural Information Processing Systems*, 33:17081–17093, 2020.
 - [15] A. Ilyas, S. Santurkar, D. Tsipras, L. Engstrom, B. Tran, and A. Madry. Adversarial examples are not bugs, they are features, 2019.
 - [16] D. P. Kingma and J. Ba. Adam: A method for stochastic optimization, 2017.
 - [17] A. Krizhevsky. Learning multiple layers of features from tiny images. Technical report, Canadian Institute for Advanced Research, 2009.
 - [18] A. Kurakin, I. J. Goodfellow, and S. Bengio. Adversarial examples in the physical world. In *Artificial intelligence safety and security*, pages 99–112. Chapman and Hall/CRC, 2018.
 - [19] F. Liao, M. Liang, Y. Dong, T. Pang, X. Hu, and J. Zhu. Defense against adversarial attacks using high-level representation guided denoiser. In *Proceedings of the IEEE Conference on Computer Vision and Pattern Recognition (CVPR)*, June 2018.
 - [20] Y. Liu, X. Chen, C. Liu, and D. Song. Delving into transferable adversarial examples and black-box attacks. *arXiv preprint arXiv:1611.02770*, 2016.
 - [21] Y. Liu, X. Chen, C. Liu, and D. Song. Delving into transferable adversarial examples and black-box attacks, 2017.
 - [22] A. Madry, A. Makelov, L. Schmidt, D. Tsipras, and A. Vladu. Towards deep learning models resistant to adversarial attacks. *arXiv preprint arXiv:1706.06083*, 2017.
 - [23] B. Ru, A. Cobb, A. Blaas, and Y. Gal. Bayesopt adversarial attack. In *International Conference on Learning Representations*, 2020.
 - [24] O. Russakovsky, J. Deng, H. Su, J. Krause, S. Satheesh, S. Ma, Z. Huang, A. Karpathy, A. Khosla, M. Bernstein, A. C. Berg, and L. Fei-Fei. ImageNet Large Scale Visual Recognition Challenge. *International Journal of Computer Vision (IJCV)*, 115(3):211–252, 2015.
 - [25] A. Shafahi, M. Najibi, M. A. Ghiasi, Z. Xu, J. Dickerson, C. Studer, L. S. Davis, G. Taylor, and T. Goldstein. Adversarial training for free! In H. Wallach, H. Larochelle, A. Beygelzimer, F. d’Alché-Buc, E. Fox, and R. Garnett, editors, *Advances in Neural Information Processing Systems*, volume 32. Curran Associates, Inc., 2019.
 - [26] K. Simonyan and A. Zisserman. Very deep convolutional networks for large-scale image recognition. In *International Conference on Learning Representations*, 2015.
 - [27] J. C. Spall. *Introduction to stochastic search and optimization: estimation, simulation, and control*, volume 65. John Wiley & Sons, 2005.

- [28] I. Sutskever, J. Martens, G. Dahl, and G. Hinton. On the importance of initialization and momentum in deep learning. In S. Dasgupta and D. McAllester, editors, *Proceedings of the 30th International Conference on Machine Learning*, volume 28 of *Proceedings of Machine Learning Research*, pages 1139–1147, Atlanta, Georgia, USA, 2013. PMLR.
- [29] C. Szegedy, W. Zaremba, I. Sutskever, J. Bruna, D. Erhan, I. Goodfellow, and R. Fergus. Intriguing properties of neural networks. *arXiv preprint arXiv:1312.6199*, 2013.
- [30] T. Tieleman, G. Hinton, et al. Lecture 6.5-rmsprop: Divide the gradient by a running average of its recent magnitude. *COURSERA: Neural networks for machine learning*, 4(2):26–31, 2012.
- [31] F. Tramer, N. Carlini, W. Brendel, and A. Madry. On adaptive attacks to adversarial example defenses. *Advances in Neural Information Processing Systems*, 33:1633–1645, 2020.
- [32] F. Tramèr, N. Papernot, I. Goodfellow, D. Boneh, and P. McDaniel. The space of transferable adversarial examples, 2017.
- [33] W. Xu, D. Evans, and Y. Qi. Feature squeezing: Detecting adversarial examples in deep neural networks. *arXiv preprint arXiv:1704.01155*, 2017.
- [34] V. Zantedeschi, M.-I. Nicolae, and A. Rawat. *Efficient Defenses Against Adversarial Attacks*, page 39–49. Association for Computing Machinery, New York, NY, USA, 2017.

A Angles between random vectors

Consider a vector space $V = \mathbb{R}^n$ and two random vectors $a = (a_1, \dots, a_n) \in \mathbb{R}^n$ and $b = (b_1, \dots, b_n) \in \mathbb{R}^n$ sampled independently from the unit sphere's surface. The process of choosing the vectors is invariant to rotations of the axes system. Therefore it's equivalent to representing a and b as $a = (1, 0, \dots, 0)$ and $b = (b'_1, \dots, b'_n)$.

The projection of b onto a is:

$$proj_a b = \frac{a \cdot b}{\|a\|} = \frac{a \cdot b}{1} = a \cdot b = 1 \cdot b'_1 + \sum_{i=2}^n 0 \cdot b'_i = b'_1$$

$$proj_a b = \frac{a \cdot b}{\|a\|} = b'_1$$

Due to symmetry, we get that $\forall_{1 \leq i, j \leq n} : \mathbb{E}(|b'_i|^p) = \mathbb{E}(|b'_j|^p)$. Additionally, for ℓ_p norm, we know that $\|b\| = (\sum_{i=1}^n |b'_i|^p)^{1/p} = 1$, therefore:

$$1 = \mathbb{E}(\sum_{i=1}^n |b'_i|^p) = \sum_{i=1}^n \mathbb{E}(|b'_i|^p) = \sum_{i=1}^n \mathbb{E}(|b'_i|^p) = n \cdot \mathbb{E}(|b'_1|^p)$$

$$\mathbb{E}(|b'_1|^p) = \frac{1}{n}$$

The angle θ between a and b satisfies the following:

$$\frac{a \cdot b}{\|a\| \|b\|} = \cos \theta$$

Since we already calculated $\frac{a \cdot b}{\|a\|}$ and we know that $\|b\| = 1$, we get:

$$\cos \theta = \frac{a \cdot b}{\|a\| \|b\|} = \frac{a \cdot b}{\|a\|} \cdot \frac{1}{\|b\|} = b'_1 \cdot \frac{1}{1} = b'_1$$

The expected value of $\cos^p \theta$ is $\mathbb{E}(|b'_1|^p) = \frac{1}{n}$. Simplifying this expression will produce an average angle of $\theta = \arccos((\frac{1}{n})^{1/p})$ for positive values of b'_1 and $\theta = \arccos(-(\frac{1}{n})^{1/p})$ for negative values of b'_1 .

$$\begin{aligned}\theta &= \arccos \left(\left(\frac{1}{n} \right)^{1/p} \right) \\ \theta &= \arccos \left(- \left(\frac{1}{n} \right)^{1/p} \right)\end{aligned}$$

For positive correlation between a and b and ℓ_2 norm (which produces an average angle of $\theta = \arccos \frac{1}{\sqrt{n}}$), we will calculate some examples for different space dimensions and their expected angle in Table 3.

Table 3: Examples for different space dimensions and the expected angle between random vectors in that dimension (for positive correlation and ℓ_2 norm).

Dimension(n)	Expected angle
2	45.0°
16	75.52°
128	84.92°
784	87.92°
3072	88.96°
196608	89.87°

Additionally, the variance is:

$$\mathbb{V}(b'_1) = \mathbb{E}(b'^2_1) - \mathbb{E}(b'_1)^2 = \mathbb{E}(b'^2_1) - 0 = \mathbb{E}(|b'_1|^2) = \frac{1}{n}$$

therefore, for higher dimensions we get smaller variance. Based on that, the probability of getting small angles between random vectors in high dimensions is much lower.

Markov's inequality states the following:

$$P(X \geq a) \leq \frac{\mathbb{E}(X)}{a}$$

for non-negative random variable X and $a > 0$.

We can use Markov's inequality to upper bound the probability of getting some angle θ between random vectors. We will use the following input $X = |b'_1|^2$, $a = \frac{t}{n}$ for integer $t > 0$ and $\mathbb{E}(|b'_1|^2) = \frac{1}{n}$:

$$P(|b'_1|^2 \geq \frac{t}{n}) \leq \frac{\mathbb{E}(|b'_1|^2)}{a} = \frac{\frac{1}{n}}{\frac{t}{n}} = \frac{1}{t}$$

It means that the probability of getting $\theta \leq \arccos \left(\left(\frac{t}{n} \right)^{1/2} \right)$ is lower than $\frac{1}{t}$. In Table 4 we can see the probability of getting different angles for dimension size of 3072.

Table 4: An upper bound for the probability of getting angles between random vectors for $n = 3072$, based on different t values.

Assigned t	Angle	Probability's upper bound ($1/t$)
1	89.96°	1.0
2	88.53°	0.5
10	86.72°	0.1
100	79.60°	0.01
350	70.27°	0.0028
1000	55.21°	0.001

In Table 4, we concluded only an upper bound for the discussed probabilities, in reality the probabilities are even lower. For example, we can experimentally calculate the angles for a large number of 100,000 pairs of random vectors of size 3072. The *minimum* angle we are getting out of the 100,000 angles is 85.29°.

B Architectures

B.1 Fully-connected architectures

In Figure 6, we can see the two fully-connected architectures used in this work. We address them as the “Shallow network” and the “Deep network”.

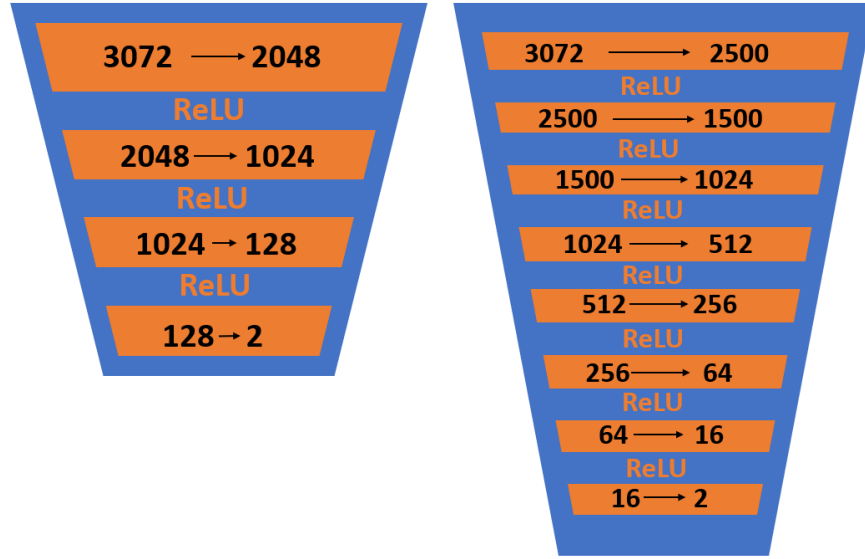


Figure 6: The architectures of the “Shallow network” (on the left) and the “Deep network” (on the right).

B.2 Convolutional architectures

Architecture A: A shallow architecture of a convolutional network:

- **Convolutional layer** [input filters: 3, output filters: 128]
kernel size: 5, stride: 2, padding: 1
- **ReLU layer**
- **Convolutional layer** [input filters: 128, output filters: 128]
kernel size: 5, stride: 2, padding: 1
- **ReLU layer**
- **Convolutional layer** [input filters: 128, output filters: 256]
kernel size: 5, stride: 2, padding: 1
- **ReLU layer**
- **Convolutional layer** [input filters: 256, output filters: 256]
kernel size: 5, stride: 2, padding: 1
- **ReLU layer**
- **Flatten**
- **Fully-connected layer** [input: 256, output: 2]

Architecture B: A deep architecture of a convolutional network:

- **Convolutional layer** [input filters: 3, output filters: 128]
kernel size: 3, stride: 1, padding: 1
- **BatchNorm layer** [filters: 128]
- **ReLU layer**
- **Convolutional layer** [input filters: 128, output filters: 128]
kernel size: 3, stride: 1, padding: 1

- **BatchNorm layer** [filters: 128]
- **ReLU layer**
- **MaxPool layer**
kernel size: 2, stride: 2, padding: 0, dilation: 0
- **Convolutional layer** [input filters: 128, output filters: 256]
kernel size: 3, stride: 1, padding: 1
- **BatchNorm layer** [filters: 256]
- **ReLU layer**
- **Convolutional layer** [input filters: 256, output filters: 256]
kernel size: 3, stride: 1, padding: 1
- **BatchNorm layer** [filters: 256]
- **ReLU layer**
- **MaxPool layer**
kernel size: 2, stride: 2, padding: 0, dilation: 0
- **Convolutional layer** [input filters: 256, output filters: 512]
kernel size: 3, stride: 1, padding: 1
- **BatchNorm layer** [filters: 512]
- **ReLU layer**
- **Convolutional layer** [input filters: 512, output filters: 512]
kernel size: 3, stride: 1, padding: 1
- **BatchNorm layer** [filters: 512]
- **ReLU layer**
- **MaxPool layer**
kernel size: 2, stride: 2, padding: 0, dilation: 0
- **Convolutional layer** [input filters: 512, output filters: 1024]
kernel size: 3, stride: 1, padding: 0
- **BatchNorm layer** [filters: 1024]
- **ReLU layer**
- **MaxPool layer**
kernel size: 2, stride: 2, padding: 0, dilation: 0
- **Flatten**
- **Fully-connected layer** [input: 1024, output: 2]

C Additional experiments

C.1 Details

The following experiments demonstrate many cases that clearly show the early transferability effect. The settings appear in Table 5. The architectures are based on Appendix B and Resnet18 [13]. Cases 1-8 consider the categories *Cat* and *Dog* of the dataset CIFAR10. Case 9 address the categories *Goldfish* and *White shark* of the dataset ImageNet.

Table 5: Possible parameters we will use in the experiments.

	Model 1	Model 2	Learning rate	Batch size
Case 1	FC Deep network	FC Deep network	1e-3	128
Case 2	FC Deep network	FC Deep network	1e-4	1024
Case 3	FC Shallow network	FC Shallow network	1e-2	128
Case 4	FC Shallow network	FC Deep network	1e-2	128
Case 5	FC Shallow network	FC Deep network	1e-3	1024
Case 6	Convolutional Architecture A	Convolutional Architecture A	1e-3	1024
Case 7	Convolutional Architecture B	Convolutional Architecture A	1e-3	128
Case 8	Resnet18	Resnet18	1e-3	16

C.2 results

In Figures 7,8,9,10,11,12,13,14, we can see the graph analysis that was mentioned in the section 3 of all the cases in Table 5.

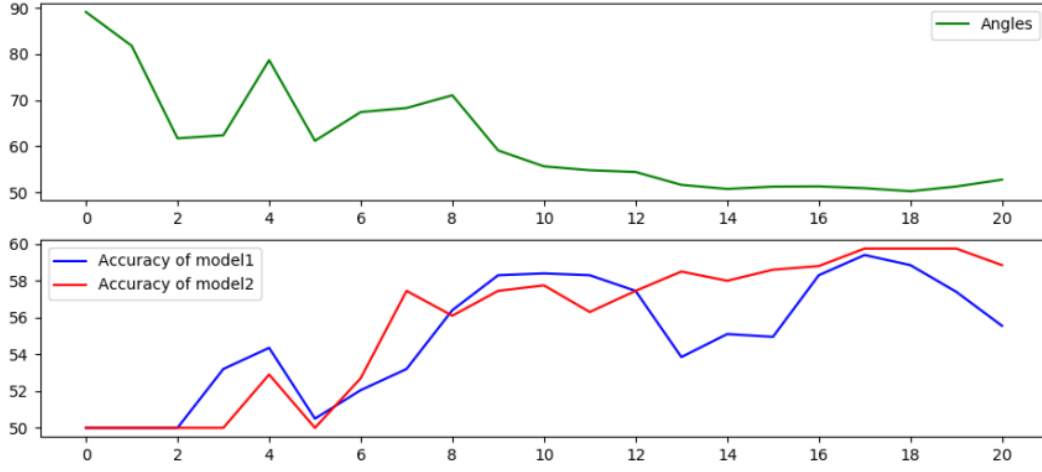


Figure 7: Early transferability - Case 1.

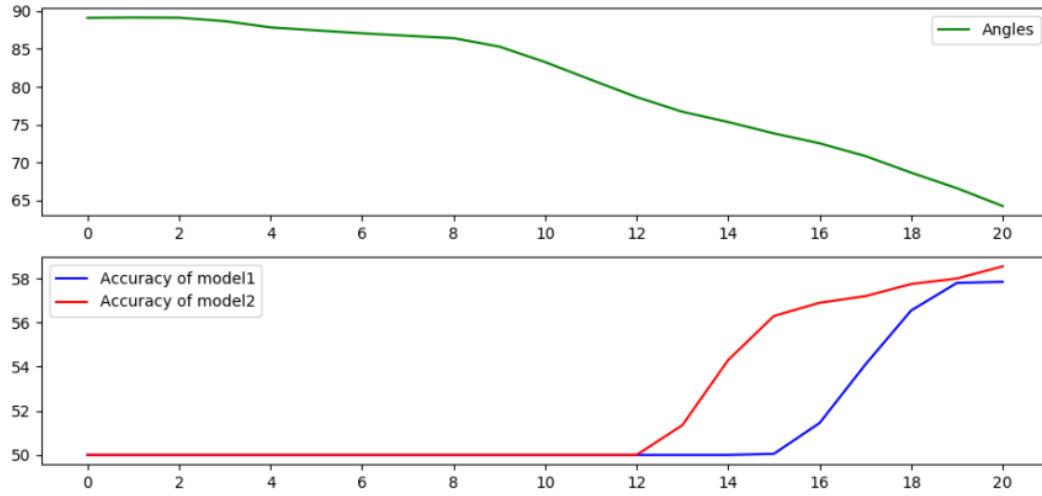


Figure 8: Early transferability - Case 2.

C.3 long-term transferability

Following section 4.5, we conduct an additional experiment using similar settings but with a different pair of categories of the dataset CIFAR10, *Cat* and *Dog*. In Figures 15 and 16, we can see a similar occurrence to the one we witnessed in section 4.5.

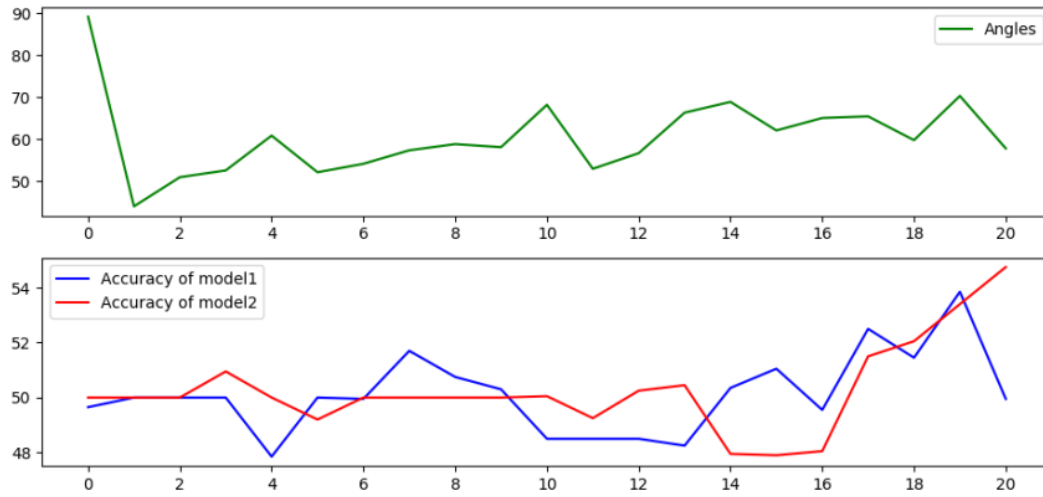


Figure 9: Early transferability - Case 3.

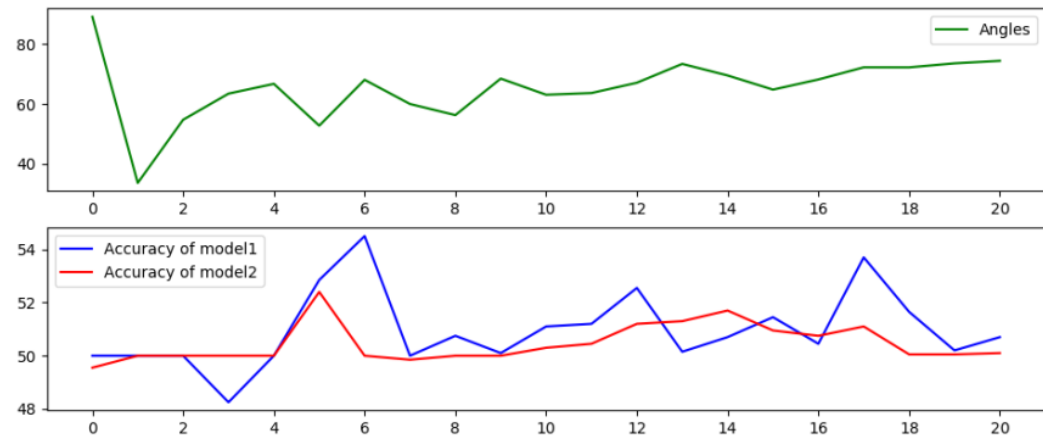


Figure 10: Early transferability - Case 4.

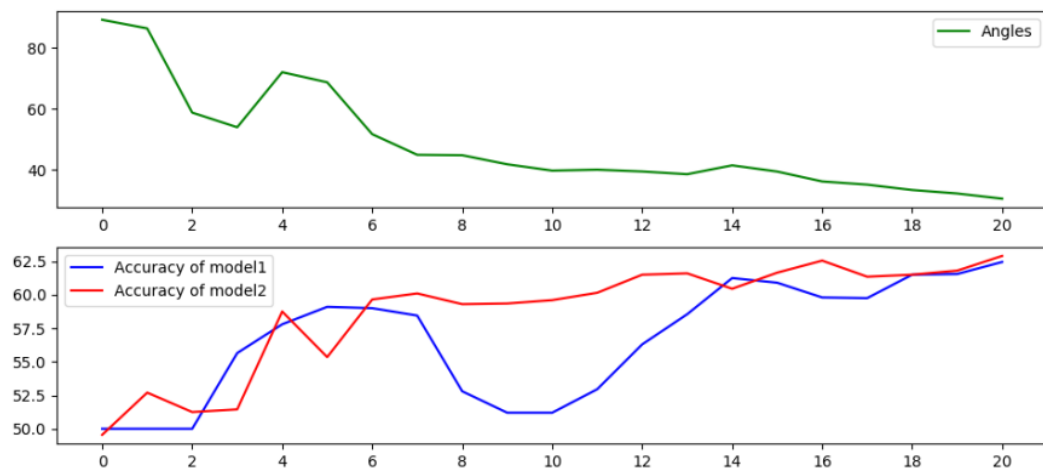


Figure 11: Early transferability - Case 5.

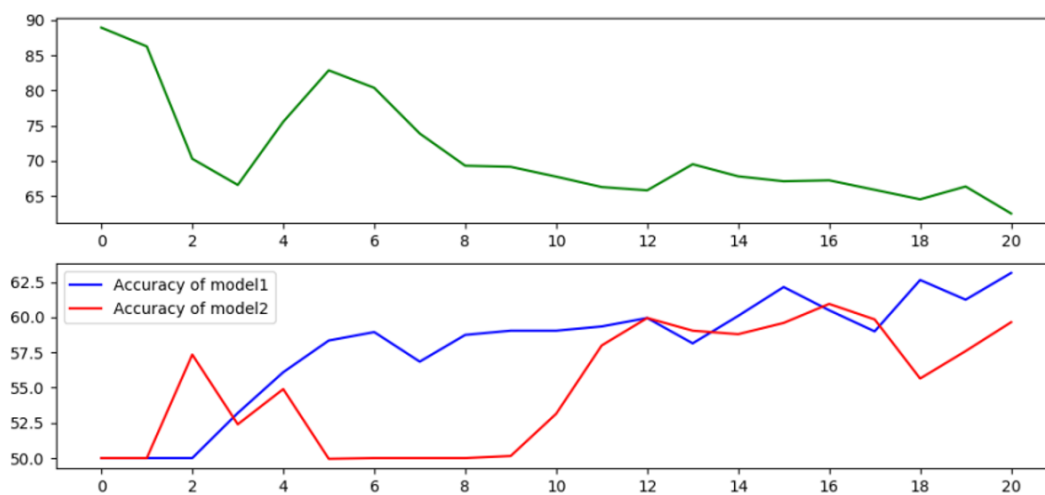


Figure 12: Early transferability - Case 6.

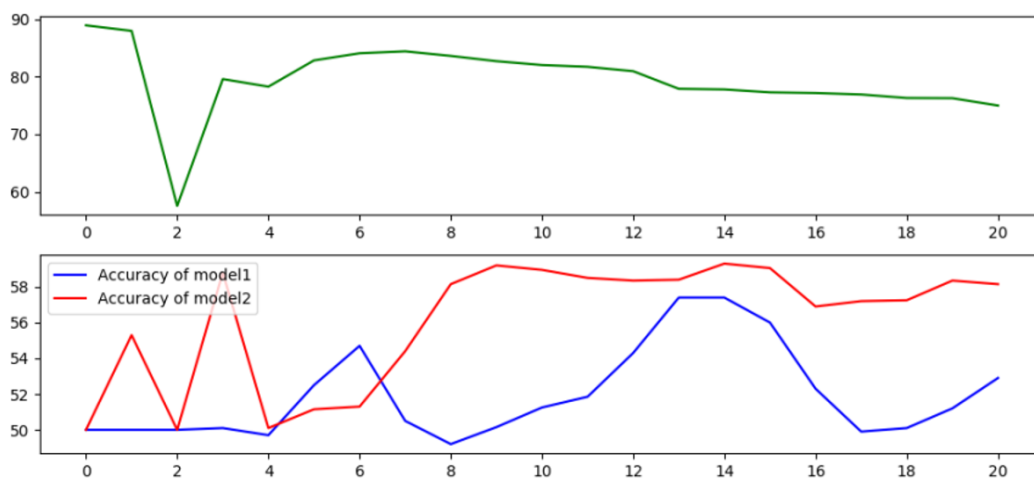


Figure 13: Early transferability - Case 7.

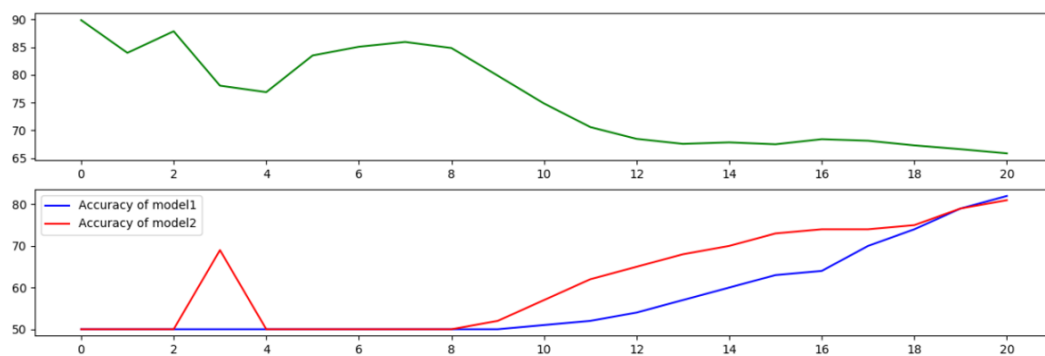


Figure 14: Early transferability - Case 8.

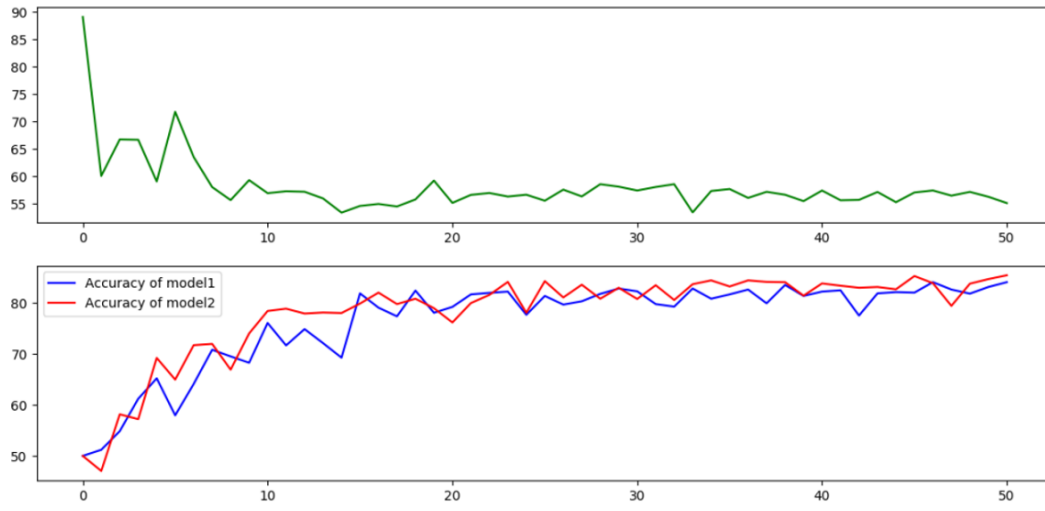


Figure 15: Long-term influence using epochs timeline. Learning rate of $1e - 2$

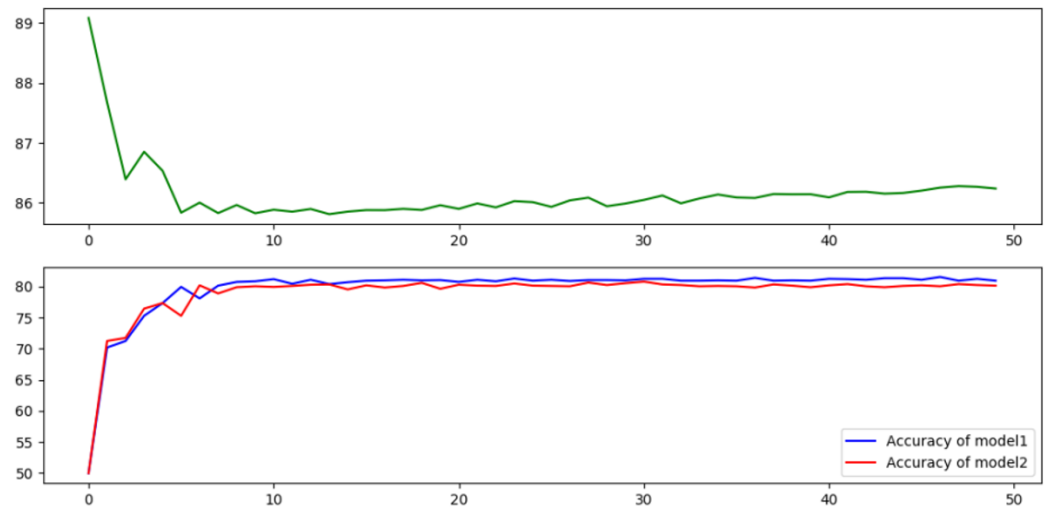


Figure 16: Long-term influence using epochs timeline. Learning rate of $1e - 4$